Clutter Rejection Techniques for Microwave Head Imaging

A. Zamani, A.M. Abbosh
School of Information Technology and Electrical Engineering
The University of Queensland
Brisbane, Australia
Email: a.zamani@uq.edu.au

***Abstract* —Microwave head imaging is a promising technique for brain injury detection. In that technique, electromagnetic waves are sent into the head by an antenna array surrounding the head and the scattered signals are processed to form an image for brain injury detection purposes. Strong wave reflections from the outer layers of the head and their overlapping with target's signals can cause a strong clutter in the received signal. This clutter can adversely affect the accuracy of reconstructed image by masking the target response. To that end, different clutter removal techniques, including average subtraction, differential approach, spatial filtering, and entropy-based filtering are investigated in this paper. Those methods are tested in a simulation environment with a realistic head model surrounded by an 8-element antenna array. The obtained results are assessed by performance metrics to compare the ability of the investigated methods in cancelling the clutter from the received signals of microwave head imaging system.**

Keywords— Clutter rejection; head imaging; microwave imaging

I. Introduction

Microwave imaging is an emerging method for brain injury detection. In that method, low-power microwave signals are transmitted towards the head and the scattered signals are recorded and processed to generate images of the head [1]. The significant difference between the dielectric properties of injured and healthy brain tissues at microwave frequencies represents the basis of microwave head imaging [2].

The outer section of the human head consists of different tissue layers, such as skin, skull, fat and muscles, which surround different internal tissues of the brain. The strong reflections from the outer layers of the head due to the high dielectric constant of those layers and time delay of the wave propagation in multilayer structures causes a clutter in the scattered signals. This clutter is strong enough to dominate the target response. To get any meaningful image that enables the successful detection of any brain injuries, the clutter should be removed without affecting the target response information. Therefore, a preprocessing technique is required to remove the clutter from the received signal.

In recent years, different clutter removal algorithms have been developed in different applications to remove the clutter effects [3]-[7]. In this paper existing clutter removal techniques are described, modified for use in head imaging and compared in the environment of microwave head imaging.

II. Clutter Removal Techniques

Five common clutter removal techniques are considered for frequency-domain, multi-static imaging systems and explained according to the head imaging environment. In the following analyses, it is assumed that N_a antennas surround the imaging domain (head) to provide N_a^2 multistatic data with N_f frequency samples. The sampled waveform transmitted by antenna i and received by antenna j is denoted by $b(i, j, n)$.

A. Average Subtraction Method

Assuming that the antennas are located at the same distance from the head boundary and that the outer layers have a uniform thickness around the head, the clutter influences does not vary with the antenna position, whilst target reflections have different impacts on each antenna. In this case, the clutter removal can be achieved by separating a constant value from the signals. One of the simple but effective methods, which support this type of clutter removal, is average subtraction [3] in which the average value of signals are considered as the reference waveform (w). The reference waveform can be easily calculated over all receivers and transmitters in each frequency sample:

$$w(n) = \frac{1}{N_a^2}\sum_{j=1}^{N_a}\sum_{i=1}^{N_a} b(i,j;\, n)\ ,\ n = 1 \text{ to } N_f \qquad (1)$$

The reference waveform is then subtracted from each antenna's signal in each frequency sample to create the clutter removed signal (*S*):

$$S(i,j;n) = b(i,j;n) - w(n)\,, \quad n = 1 \text{ to } N_f \tag{2}$$

Applying the averaging process over frequency samples effectively removes the artifact of each frequency dataset, according to the variation of the clutter behavior with frequency. However, the assumption of uniform structure of different layers causes the presence of ghost targets in the reconstructed image using this method.

B. Differential Approach – type A

Assuming constant thicknesses of the layers in front of two adjacent antennas rather than the whole imaged domain provides differential clutter removal method [4]. In this method, the clutter is removed by subtracting two adjacent traces:

$$S(i,j;n) = b(i,j;n) - b(i-1,j-1;n) \tag{3}$$

for $i,j = 1$ to $\frac{N_a}{2}$ with $i-1 = j-1 = N_a$ for $i,j = 1$

$$S(i,j;n) = b(i,j;n) - b(i+1,j+1;n) \tag{4}$$

for $i,j = \frac{N_a}{2}+1$ to N_a with $i+1 = j+1 = 1$ for $i,j = N_a$.

Generating ghost targets and/or false targets due to the subtraction process is the disadvantage of this method.

C. Differential Approach – type B

The multiple reflections can be assumed identical in symmetrical antenna locations on the left and right sides of the head, due to the anatomically symmetrical structure of the human head over the left and right sides. Therefore, another type of differential approach can be developed by performing subtraction over two symmetrical antennas [5]:

$$S(i,j;n) = b(i,j;n) - b(N_a+2-i, N_a+2-j;n) \tag{5}$$

for $i,j = 1$ to N_a with $N_a+1 = \frac{N_a}{2}+1$ for $i,j = 1$ and $\frac{N_a}{2}+1 = 1$ for $i,j = \frac{N_a}{2}+1$.

Subtracting the signals from symmetrical antennas generates mirrored ghost targets, which can adversely affect the quality of the reconstructed images.

D. Spatial Filtering

From the spatial point of view and by assuming equal thickness of the outer layers, reflected signals from the outer layer are either constant or have low-spatial frequency values, whereas the reflected signals from the target inside the imaged domain are variant from the antennas' perspective. Therefore, low-pass finite-impulse-response or spatial delay-line canceler filters can be used to suppress the outer-layer reflections by removing the spatial zero and low frequency components of the signals corresponding to skin reflections.

To that end, the received time or frequency domain signals are transformed to their angular spectrum to generate reference waveform (w):

$$w(u,v;n) = \iint_s b(x,y;n)e^{-i2\pi(xu+yv)}dxdy\,, \tag{6}$$

where u and v are spatial frequencies and (x, y) is the corresponding location of the receiver antennas.

A spatial notch filter [6] is then applied to the reference waveform to filter out the spatially zero and low frequency signals:

$$H_{NF}(n) = \frac{1-e^{-i2\pi n}}{1-\alpha e^{-i2\pi n}}\,, \tag{7}$$

in which $0<\alpha<1$ determines the width of the filter notch.

This method, however, also affects the target's signals and a careful consideration is needed to repair the data. In addition, finding the optimum value for α needs initial knowledge about the properties and dimensions of the layers, and thus, makes this method difficult to use.

E. Entropy-based Filtering

This method is an advanced version of simple time-gating [7] method in which the clutter was removed by filtering the first part of the received signal in the time domain. To address the time-gating problems, such as time overlapping and data removal of shallow-targets, an entropy-based metric to discriminate between clutter and target signals was introduced [8]. In this case, the signals over a tolerance threshold are considered as a clutter and thus removed:

$$S(i,j;n) = \begin{cases} 0 & e^{H_\alpha(n)} \geq N_0 \\ b(i,j;n) & otherwise \end{cases}\,, \tag{8}$$

where $1<N_0<N_a^2$ is the entropy threshold, which is suggested to be half of the number of received signals, and H_α is the αth-order Renyi entropy [9]:

$$H_\alpha(n) = \frac{1}{1-\alpha} log\left(\sum_{j=1}^{Na}\sum_{i=1}^{Na}[P(i,j;n)]^\alpha\right)\,, \tag{9}$$

where

$$P(i,j;n) = \frac{|b(i,j;n)|^2}{\sum_{j=1}^{Na}\sum_{i=1}^{Na}|b(i,j;n)|^2}\,, \tag{10}$$

which satisfies $P(i,j;n) \geq 0$ and $\sum_{j=1}^{Na}\sum_{i=1}^{Na}P(i,j;n) = 1$.

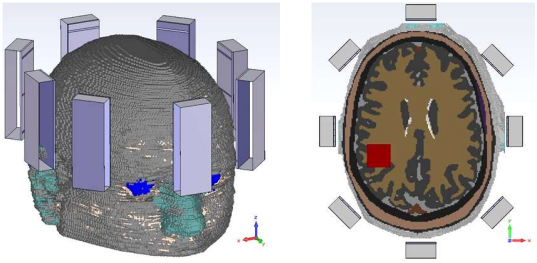

Fig. 1. Simulation setup of head imaging system. The red rectangle shows an assumed brain injury.

Applying the entropy-based filtering in the frequency domain makes it resilient to time delay and overlapping. However, due to the frequency response overlapping, entirely eliminating a frequency component also erases a portion of the target data.

III. Imaging Results

To investigate the effectiveness of the aforementioned clutter removal techniques in microwave head imaging, they are applied to a set of recorded data using realistic MRI-based head model [10] in CST Microwave Studio. The head phantom model consists of a multilayer outer structure (skin, skull, fat, and muscle) and 17 types of overlapped internal tissues with their actual electrical properties across the band of interest. To emulate the scenario of a brain injured (bleeding) patient, a small volume of blood with dimensions of 2 × 2 × 2 cm3 is placed inside the model. To collect data, a circular antenna array consisting of 8 compact ultra-wideband antennas [11] is positioned around the head as shown in Fig. 1. In this configuration, all the antennas act as both transmitter and receiver. In every step, UWB signals are transmitted by each of the antennas, while all the other antennas receive the scattered signals. The swept frequency covers the band 1.1-3.2 GHz. The received signals are recorded in every 60 MHz sample.

The aforementioned clutter removal methods are then applied to the captured data as a preprocessing step of a modified frequency-based algorithm [12] to form a two dimensional image from the clutter removed waveforms. The imaging algorithm calculates the intensity of the power, $I(x, y)$ inside the imaging region using Bessel function of the first kind $J_1(k\rho)$:

$$I(x,y) = \left\| \sum_{n=1}^{Nf} \sum_{j=1}^{Na} \sum_{i=1}^{Na} S(i,j,n) J_1^2(k\rho) e^{i2(k\rho+\varphi)} \right\|, \qquad (11)$$

where k is the wavenumber inside the imaging domain and (ρ, φ) is the distance and the angle between a transmitter and a receiver by selecting a point-scatterer at (x, y) inside the imaging region.

The reconstructed images by using different clutter removal methods are shown in Fig. 2. Fig. 2 (a) shows the obtained

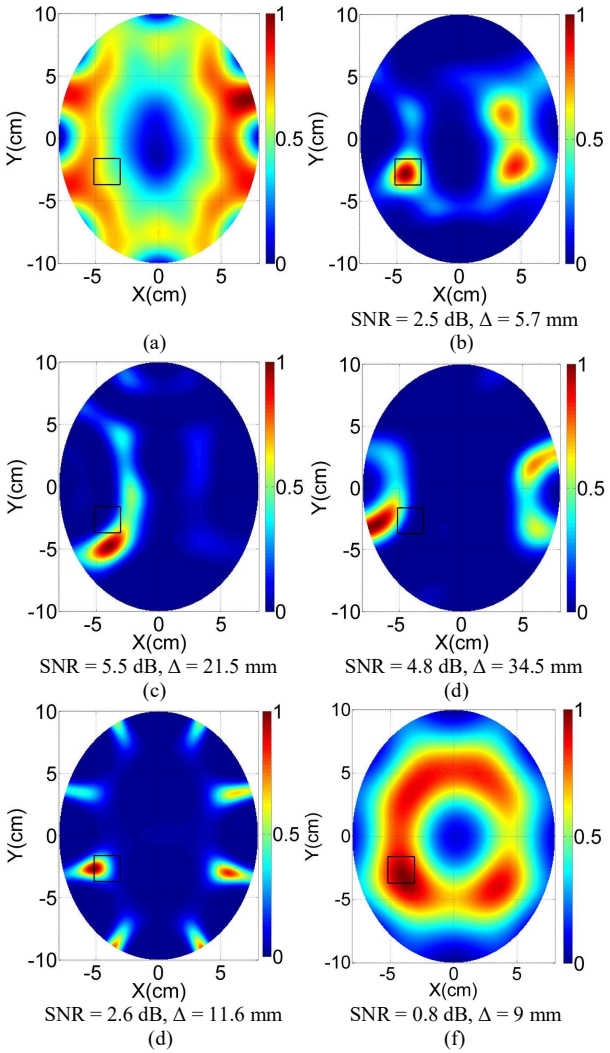

Fig. 2. Reconstructed images (a) without applying clutter removal techniques, and after using (b) average subtraction, (c) differential approach-A, (d) differential approach-B, (e) spatial filtering (α=0.9), and (f) entropy-based filtering. Black rectangles show the exact location of the target.

image without applying any clutter removal technique. This image demonstrates how the target is completely masked by the strong clutter. Visual comparison shows that average subtraction (Fig. 2 (b)) and entropy-based filtering (Fig. 2 (f)) methods can exactly localize the target, though the ghost targets indicate that these methods do not completely remove the clutter. The resultant effect of not-filtered frequencies in entropy-based filtering is a halo along the target location in the reconstructed image. Differential approaches (Fig. 2 (c) and (d)) and spatial filtering (Fig. 2 (e)) have small errors in locating the target, which can be interpreted as the effect of these methods on the target signals. In addition, the reconstructed images are affected by ghost targets. The resulted image of spatial filtering is for α=0.9 which is the best value for α based on trial-and-error approach on the resultant images.

To numerically compare the performance of the explained methods and their effect on the obtained image, the signal-to-noise ratio (*SNR*) and distance to center (Δ) parameters are calculated for each constructed image:

$$SNR = 10\, log_{10}\left(\frac{I_t - I_b}{C_b}\right) \quad dB \tag{12}$$

$$\Delta = \|p - \alpha\| \tag{13}$$

where I_t and I_b in (12) are the mean values of the detected target and background regions, respectively, and C_b is the standard deviation of the background. While, α and p in (13) are real center and center of the detected target, respectively.

Higher values of SNR for a reconstructed image using a certain algorithm means better clutter removal and thus more accurate detection, while lower Δ means that the clutter removal algorithm has lower effect on the target's data. The above mentioned parameters are shown under the images in Fig. 2. As expected, the reconstructed images by average subtraction and entropy-based filtering methods have the lowest distance to center and SNR values. Differential approaches on the other hand provide high SNR values, but with significant errors (large Δ), which means these methods make the most impact on the target's data.

IV. Conclusion

Different clutter removal techniques have been reviewed and investigated for multi-static microwave head imaging in frequency domain. The different methods have been modified to be integrated into a multi-static frequency-domain imaging algorithm. The performances of the investigated methods have been tested on a realistic head model with multiple outer layers in a full-wave simulation environment. The signal-to-noise and distance to center metrics have been calculated for each reconstructed image to compare the effectiveness of each method in removing the clutter from the recorded signals. The obtained results show that all of the methods can reveal the target in the image. However, they don't cancel the clutter completely (average subtraction and entropy-based) or significantly affect the target's signal (differential approaches and spatial filtering). Thus, future research should focus on developing an algorithm that is able to remove the clutter without degrading the target's response.

References

[1] B.J. Mohammed, A.M. Abbosh, S. Mustafa, D. Ireland, "Microwave System for Head Imaging," IEEE Trans. Instrum. Meas., vol. 63, no. 1, pp. 117-123, Jan. 2014.

[2] A.T. Mobashsher, A.M. Abbosh, Y. Wang, "Microwave System to Detect Traumatic Brain Injuries Using Compact Unidirectional Antenna and Wideband Transceiver With Verification on Realistic Head Phantom," IEEE Trans. Microw. Theory Techn., vol. 62, no. 9, pp. 1826-1836, Sept. 2014.

[3] X. Li and S.C. Hagness, "A confocal microwave imaging algorithm for breast cancer detection," IEEE Microw. Compon. Lett., IEEE , vol. 11, no. 3, pp. 130-132, March 2001.

[4] M. Klemm, J. A. Leendertz, D. Gibbins, I. J. Craddock, A. Preece, and R. Benjamin, "Microwave radar-based differential breast cancer imaging: Imaging in homogeneous breast phantoms and low contrast scenarios," IEEE Trans. Antennas Propag., vol. 58, no. 7, pp. 2337–2344, Jul. 2010.

[5] S. Mustafa, B. Mohammed, and A.M. Abbosh, "Novel Preprocessing Techniques for Accurate Microwave Imaging of Human Brain," IEEE Antennas Wireless Propag. Lett., vol. 12, pp. 460-463, 2013.

[6] Yeo-Sun Yoon, M.G. Amin, "Spatial Filtering for Wall-Clutter Mitigation in Through-the-Wall Radar Imaging," IEEE Trans. Geosci. Remote Sens., vol. 47, no. 9, pp. 3192-3208, Sept. 2009.

[7] M. Sarafianou, I.J. Craddock, T. Henriksson, "Towards Enhancing Skin Reflection Removal and Image Focusing Using a 3-D Breast Surface Reconstruction Algorithm," IEEE Trans. Antennas Propag., vol. 61, no. 10, pp. 5343-5346, Oct. 2013.

[8] Y. Zhang, P. Candra, W. Guoan, X. Tian, "2-D Entropy and Short-Time Fourier Transform to Leverage GPR Data Analysis Efficiency," IEEE Trans. Instrum. Meas., vol. 64, no. 1, pp. 103-111, Jan. 2015.

[9] R.G Baraniuk, P. Flandrin, A.J.E.M. Janssen, O.J.J. Michel, "Measuring time-frequency information content using the Renyi entropies," IEEE Trans. Inf. Theory, vol. 47, no. 4, pp. 1391-1409, May 2001.

[10] I.G. Zubal, et al., "Computerized three-dimensional segmented human anatomy", Medical Physics, vol. 21, no. 2, pp. 299-302, 1994.

[11] A.T. Mobashsher and A.M. Abbosh, "Slot-Loaded Folded Dipole Antenna with Wideband and Unidirectional Performance for L-Band Applications," IEEE Antennas Wireless Propag. Lett., vol. 13, pp. 798-801, 2014.

[12] A. Zamani, S.A. Rezaeieh, A.M. Abbosh, "Lung cancer detection using frequency-domain microwave imaging," Electronics Letters , vol. 51, no. 10, pp. 740-741, 2015.